Revision_1

A neutron diffraction study of boussingaultite, $(NH_4)_2[Mg(H_2O)_6](SO_4)_2$

G. Diego Gatta, Giorgio Guastella, Alessandro Guastoni, Valentina Gagliardi, Laura Cañadillas-Delgado and Maria Teresa Fernandez-Diaz

Running title: Crystal chemistry of boussingaultite

Abstract, Keywords
Introduction
Sample description and occurrence
Experimental methods and Results
1) **Gravimetric determination of sulphates**
2) **EDTA titrimetric determination of magnesium**
3) **Determination of fluorine and chlorine by ion selective electrode**
4) **Determination of water content by heating**
5) **Determination of minor elements by inductively coupled plasma atomic emission spectroscopy (ICP-AES) and air-acetylene flame atomic emission spectrometry (FAES)**
   - ***5.1) Determination of REE concentration by ICP-AES***
   - ***5.2) Determination of other minor elements concentration by ICP-AES***
6) **Indirect gravimetric determination of ammonium as (NH_4,Rb,Cs,K) tetraphenylborate**
7) **Determination of CHN**
8) **Single-crystal neutron diffraction**
   - ***8.1) Neutron data collections and treatments***
   - ***8.2) Neutron structure refinements***

Discussion and implications
Acknowledgements
References
Figures/Tables

Corresponding author: G. Diego GATTA
Dipartimento di Scienze della Terra, Università degli Studi di Milano
Via Botticelli 23, I-20133 Milano, Italy
Tel. +39 02 503 15607, Fax +39 02 503 15597, E-Mail: diego.gatta@unimi.it

Manuscript submitted to American Mineralogist

A neutron diffraction study of boussingaultite, $(NH_4)_2[Mg(H_2O)_6](SO_4)_2$

G. Diego Gatta[1], Giorgio Guastella[2], Alessandro Guastoni[3], Valentina Gagliardi[4], Laura Cañadillas-Delgado [5] and Maria Teresa Fernandez-Diaz[6]

[1]Dipartimento di Scienze della Terra, Università degli Studi di Milano,
Via Botticelli 23, I-20133 Milano, Italy
[2]Agenzia delle Accise, Dogane e Monopoli, DTI – Lombardia, Ufficio Antifrode - Sezione Laboratori,
Via Marco Bruto 14, I-20138 Milano, Italy
[3]Dipartmento di Geoscienze, Università degli Studi di Padova,
Via G. Gradenigo 6, I-35131, Padova, Italy
[4]Istituto Gemmologico Italiano, Piazza San Sepolcro 1, I-20123 Milano, Italy
[5]Institut Laue-Langevin, 71 Avenue des Martyrs, F-38000 Grenoble, France

Abstract

The crystal structure and the chemical composition of boussingaultite from Pécs-Vasas, Mecsek Mountains, South Hungary, were investigated by single-crystal neutron diffraction (at 20 K) along with a series of chemical analytical techniques (*i.e.*, gravimetric determination of sulphates, EDTA titrimetric determination of magnesium, ion selective electrode for F and Cl, indirect gravimetric determination of ammonium as (NH_4,Rb,Cs,K) tetraphenylborate, inductively coupled plasma atomic emission spectroscopy for REE and other minor elements, elemental analysis for C, N and H content, high-*T* mass loss for H_2O content). The concentration of more than 50 elements was measured. The experimental formula of the boussingaultite of this study is: $[(NH_4)_{1.77}K_{0.22})_{\Sigma 1.99}[(Mg_{0.95}Mn_{0.06})_{\Sigma 1.01}(H_2O)_{5.7}](SO_4)_{1.99}$. The neutron refinement confirms that the structure of boussingaultite is built up by: isolated $Mg(H_2O)_6$-octahedra, along with isolated NH_4- and SO_4-tetrahedra connected by a complex H-bonds network. Mg^{2+} is completely solvated by H_2O molecules, in a typical octahedral bonding configuration. All the seven independent oxygen sites of the structure are involved in H-bonds, as *donors* or as *acceptors*. The geometry of all the H_2O molecules, bonded to Mg, is in line with what usually observed in crystalline compounds. The H_2O molecules show moderate-strong H-bonds, with $H\ldots O_{acceptor}$ and $O_{donor}\ldots O_{acceptor}$ ranging between 1.72-1.87 Å and 2.70-2.84 Å, respectively, along with O_{donor}-$H\ldots O_{acceptor}$ angles between 168-178°. The four independent *N*-*H*…*O* bonds show $H\ldots O_{acceptor}$ and $N_{donor}\ldots O_{acceptor}$ distances ranging between 1.81-2.00 and 2.84-2.98 Å, respectively, with *N*-*H*…*O* angles between 158-176°. All the H-bonds of the H_2O molecules and of the NH_4-group involve the oxygen sites of the SO_4-group as *acceptors*: the SO_4-group is, therefore, the "bridging unit" between the NH_4 and the $Mg(H_2O)_6$ units, *via* H-bonds. The structure refinement of this study proved, unambiguously, that the partial K^+ *vs.* NH_4^+ replacement generates a local disorder. K lies

at the *N* site, and its bonding configuration is described with a distorted polyhedron with CN=8. However, the K^+ *vs.* NH_4^+ replacement implies a change in the configuration of the SO_4-tetrahedron, through a sort of rotation of the polyhedron. This is the first evidence of a partial picromerite component in the boussingaultite structure, which gives rise to a local disorder likely due to the significantly different bonding configurations of the two cations. The refinement proved also that Mn^{2+} replaces Mg^{2+} at the *Mg* site. No evidence of distortion of the octahedron is observed in response to such a replacement, but the fraction of Mn^{2+} is modest. An analysis of previous Raman and IR findings is provided, compared with the experimental results of this study.

Keywords: Boussingaultite, sulphates, neutron diffraction, crystal chemistry, hydrogen bonding.

Introduction

Boussingaultite is a magnesium ammonium sulphate hexahydrate, with ideal chemical formula usually given as $(NH_4)_2Mg(SO_4)_2{\cdot}6H_2O$. It is a rare mineral, which occurs as sublimate formed under fumarolic conditions, geysers, or from coal gas at burning coal-dumps (*e.g*., Cipriani 1959; Larsen and Shannon 1920; Shimobayashi et al. 2011). It is found as stalactites and incrustations, more rarely as monoclinic crystals (short prismatic [001] with {001} prominent). Boussingaultite is one of a wide number of isomorphous compounds (mainly synthetic) called "Tutton's salts" (Tutton 1900, 1905), a family of double salts with the formula $A^+_2B^{2+}(SO_4)_2(H_2O)_6$ (sulphates) or $A^+_2B^{2+}(SeO_4)_2(H_2O)_6$ (selenates), with A^+: K, Rb, Cs, Tl or NH_4, B^{2+}: Mg, V, Cr, Mn, Fe, Co, Ni, Cu, Zn or Cd. Focusing on natural compounds, boussingaultite belongs to the picromerite group of minerals, with picromerite ($K_2Mg(SO_4)_2{\cdot}6H_2O$), nickelpicromerite ($K_2Ni(SO_4)_2{\cdot}6H_2O$), nickelboussingaultite ($(NH_4)_2Ni(SO_4)_2{\cdot}6H_2O$), mohrite ($(NH_4)_2Fe(SO_4)_2{\cdot}6H_2O$), katerinopoulosite ($(NH_4)_2Zn(SO_4)_2{\cdot}6H_2O$), and cyanochroite ($K_2Cu(SO_4)_2{\cdot}6H_2O$). Tutton's salts structure is monoclinic, usually described in the space group $P2_1/a$ with a~9.0-9.4, b~12.3-12.9, c~6.0-6.4 Å and β~104-107°, Z = 2. The first general structure model was reported by Hofmann (1931), followed by a series of re-investigations for any specific compound of the family based on X-ray or even neutron diffraction, on single-crystal or polycrystalline sample. Concerning boussingaultite, a few crystallographic studies were performed but all on the synthetic counterpart with ideal composition (Margulis and Templeton 1962; Montgomery and Lingafelter 1964; Maslen et al. 1988). As a matter of fact, all the mineralogical databases refer only to the structural models of the synthetic analogous. The building units of the boussingaultite structure consist of isolated $Mg(H_2O)_6$-octahedra, NH_4- and SO_4-tetrahedra connected by a network of H-bonds, which must plays a fundamental role on the stability of the crystalline edifice. In this light, the chemical

formula of boussingaultite is better written as $(NH_4)_2[Mg(H_2O)_6](SO_4)_2$, rather than $(NH_4)_2Mg(SO_4)_2 \cdot 6H_2O$ as commonly reported. The presence of NH_4-group generates a different bonding configuration with respect to other members of the picromerite group, in which *e.g.* K^+ replaces NH_4^+ (Bosi et al. 2009). A thorough comparative crystal-chemical study of a series of synthetic compounds with general formula $K_2[B^{2+}(H_2O)_6](SO_4)_2$, with B^{2+} = Mg, Fe, Co, Ni, Cu, and Zn, was reported by Bosi et al. (2009).

An additional limitation of the literature data on (natural) boussingaultite concerns the chemical composition of this mineral based on modern standards. Only a few chemical analyses are available, and the reference one is often that reported by Larsen and Shannon (1920) (with wt.% oxide equals to 98.3 wt%).

There is a raising interest on boussingaultite, or its synthetic counterpart, generated by some potential industrial and agricultural utilization of this material, following the operational principles of circular economy for sustainable development. For example, the global demand for agricultural fertilizer by nutrient from the quaternary system $(NH_4)_2SO_4$-$MgSO_4$-K_2SO_4-H_2O is increasing drastically (*e.g.*, the world capacity for producing ammonia + phosphoric acid + potash increased from 292 Mt on 2016 to 316 Mt on 2021; F.A.O. 2019). This leads to the requirement of the new technology for producing an increasing mass of fertilizers: soluble crystalline precipitates (among those, boussingaultite) from industrial waste sludge, as null by-product of polymers manufacturing digested to retrieve the rubber by using sulphuric acid, are used as source of S, N, K and Mg (*e.g.*, Taweepreda 2013; Li et al. 2020). A null by-product becomes a second raw material. In addition, boussingaultite (along with other Tutton's salt) is one of the potential materials suitable for strong energy absorption by solar collectors: energy required for domestic heating and hot-water supply could be "stored" in reversible transformations, *e.g.* in chemical reactions or in phase transitions (*e.g.*, Gronvold and Meisingset 1982; Lim and Lee 2010). Salt hydrates, and among those even Tutton's salts, have relatively low dehydration or melting temperatures, representing some among the most promising materials for this purpose. Furthermore, Highfield et al. (2012) reported the role of boussingaultite in the activation of serpentine for CO_2 mineralization by flux extraction of soluble magnesium salts using ammonium sulphate.

Considering the capacity of the Tutton's salt structure to allocate a series of cations at the A^+ and B^{2+} site, and the presence in nature of isomorphic minerals of boussingaultite in which Mg^{2+} is replaced by Ni^{2+} (*e.g.*, nickelboussingaultite) or in which NH_4^+ is replaced by K^+ (*e.g.*, picromerite), the aim of this study is a reinvestigation of the crystal chemistry of a natural boussingaultite (from Pécs-Vasas, South Hungary) on the basis of a multi-methodological approach based on single-crystal neutron diffraction and a series of chemical analytical techniques in order: *a*) to unveil potential replacement

mechanisms at the A^{+} and B^{2+} occurring in nature and not described so far, and *b)* to describe unambiguously the location and the anisotropic displacement regime of the proton sites, the geometry of the NH_4-group along with the complex H-bonding configuration in the structure of boussingaultite.

Sample description and occurrence

The sample of boussingaultite used for this study belongs to the mineral collection of the Museum of Mineralogy of the University of Padova (catalogue number MM6606). The hand specimen is made by an aggregate of whitish, colourless, platy-tabular millimetric crystals collected at Pécs-Vasas, Mecsek Mountains, South Hungary (Szakáll and Kristály 2008). Pécs-Vasas is an abandoned coalmine with a large open pit located near Köves Hill. Coal ores of Jurassic age occur within sandstones, claystones, mudstone sedimentary layers and carbonatic rocks. Pécs-Vasas coalfields is the type locality for ammoniomagnesiovoltaite [$(NH_4)_2Mg^{2+}_5Fe^{3+}_3Al(SO_4)_{12}\cdot 18H_2O$, Szakáll et al. 2012] and kollerite [$(NH_4)_2Fe^{3+}(SO_3)_2(OH)\cdot H_2O$, Ende et al. 2021). Several others NH_4, Al, Fe, Mg, Ca and Fe-bearing sulphates were found in the coal dumps of Pécs-Vasas. Most of them occur as euhedral, idiomorphic millimetric crystals, formed by the spontaneous burning and combustion of coal. The most interesting and uncommon NH_4-bearing sulphate minerals, at this locality, are ammonioalunite and adranosite (Szabó et al. 2015), ammoniojarosite, clairite, efremovite, godovikovite, koktaite, mascagnite, mohrite and tschermigite (Szakáll and Kristály 2008). Ammonium sulphates are often accompanied by other more common sulphates, such as alunogen, butlerite, halotrichite, pickeringite, copiapite, gypsum, hexahydrite, kieserite, metavoltine and voltaite. The formation of a relevant number of N-bearing sulphates and sulphites can be explained by the decay of the organic matter of coal, which also contain abundant pyrite and marcasite. These iron sulphides are the source of sulphur oxides, from which sulphates are formed.

Experimental methods and Results

1) Gravimetric determination of sulphates

A mass of 150-200 mg of sample was placed in a 400 ml beaker; then, 200 ml of water and 1 ml of concentrated hydrochloric acid were added. The clear solution was heated to boiling and 10 ml of 10% barium chloride solution was then added dropwise. The beaker was covered with a clockglass and was heated below the boiling point for 4 hours. The precipitate was then filtered and washed with 150 ml of hot water. A filter was placed in a pre-weighted platinum capsule (m1) and dried at 105°C for 1 hour. The filter was then completely incinerated on a Bunsen burner, and the platinum capsule

was heated at 800°C until a constant weight (m2) was measured. The different of weigh (m2 - m1) is the total SO_3 content of the mineral, expressed as $BaSO_4$. The measured fraction of SO_3 was 44.2(2) wt%.

2) EDTA titrimetric determination of magnesium

A mass of 100-150 mg of sample were placed in a 200 ml beaker, and then diluted to 100 ml with water. After complete dissolution, 10 ml of buffer solution (pH 10 mix ammonium chloride/ammonia) were added, along with 5 ml of hydroxylammonium chloride (3% solution), 1 ml of ammonium sulphide (20% solution) and 3-4 drops of *Eriochrome black-T* solution (2gr/l in ethanol). The solution was then titrated with standard solution of EDTA (ethylenediaminetetraacetic acid) 0.01 M. The end point was reached when the reddish purple colour of the solution altered to blue or green. The total volume of the added EDTA is proportional to the average content of magnesium in the mineral. The measured fraction of MgO was 10.6(2) wt%.

3) Determination of fluorine and chlorine by ion selective electrode

A mass of 20 mg of sample was placed in a 50 ml plastic test tube, along with 15 ml of water and 0.5 ml of nitric acid 1M. 2-3 ml of total ionic strength adjustment buffer (*TISAB III* solution) were added to the clear solution, and then diluted to 20 ml with water. Fluorine content was determined using the *perfectION* Combination Fluoride Ion Selective Electrode (by *Mettler Toledo*), adopting the conventional method of standard addition. Solutions of fluorine from 0.1 to 5.0 mg/l were prepared by Certified Reference Material - CRM 1000 mg/l of fluorine. The resulting F fraction was < 0.01 wt% (uncertainty not determined).

A mass of 40 mg of sample was placed in a 50 ml plastic test tube, along with 15 ml of water and 0.5 ml of nitric acid 1M. 2-3 ml of ionic strength adjustment solution (*perfectION ISA solid state ISE*) were added to the clear solution, then diluted to 20 ml with water. Chlorine content was determined using the *perfectION* Combination Chloride Ion Selective Electrode (by *Mettler Toledo*), adopting the conventional method of standard addition. Solutions of chlorine from 2 to 10 mg/l were prepared by CRM 1000 mg/l of chlorine. The resulting Cl fraction was < 0.1 wt% (uncertainty not determined).

4) Determination of water content by heating

A mass of 400-500 mg of sample was placed in a quartz crucible with lid and gradually heated (10°C/min) in a muffle furnace from ambient temperature up to 200°C. Assuming that the mass loss

represents the total amount of H_2O, the estimated H_2O fraction of the boussingaultite sample was 28.4(2) wt%.

5) Determination of minor elements by inductively coupled plasma atomic emission spectroscopy (ICP-AES) and air-acetylene flame atomic emission spectrometry (FAES)

All determinations (excluding caesium) were performed in axial view mode for REE, and radial view mode for the other minor elements, with a *Perkin Elmer Optima 7000DV* ICP-AES spectrometer. Caesium concentration was measured with a *Varian SpectrAA 220FS* air-acetylene flame atomic emission spectrometer.

5.1) ***Determination of REE concentration by ICP-AES***

A mass of 50 mg of boussingaultite was placed in a 50 ml volumetric flask, along with 25 ml of water and 5 ml of nitric acid 1M. The resulting clear solution was then diluted with water. A calibration protocol was performed with a blank solution and a series of *ad hoc* solutions with REE concentration from 0.001 to 0.050 mg/l for each element (using CRM multi elemental standard mix for ICP). Results and instrumental parameters are listed in Table 1.

5.2) ***Determination of other minor elements concentration by ICP-AES***

The determination of the non-REE minor elements was performed using two different protocols, the second one devoted only to the Cs concentration, described below:

i) 5-100 mg of sample was placed in a 50 ml volumetric flask, 25 ml of water, 5 ml of nitric acid 1M and 5 ml of scandium solution 100 mg/l were added. The resulting clear solution was diluted with water. A calibration protocol was performed with a blank solution and a series of *ad hoc* solutions with concentration from 0.001 to 0.050 mg/l for each element (using CRM multi elemental standard mix for ICP). Results and instrumental parameters are listed in Table 2.

ii) A mass of 100-200 mg of sample was placed in a 50 ml volumetric flask, along with 25 ml of water, 5 ml of nitric acid 1M and 300 mg of potassium nitrate. The clear solution was then diluted with water. A calibration protocol was performed with a blank solution and a series of *ad hoc* solutions prepared with CRM multi elemental standard mix for ICP, containing 100

mg/l of Cs (5 solutions from 1 mg/l to 20 mg/l). Results and instrumental parameters are listed in Table 2.

6) Indirect gravimetric determination of ammonium as (NH_4,Rb,Cs,K) tetraphenylborate

A mass of 100-150 mg of boussingaultite was placed in a 200 ml beaker and diluted to 50 ml with water. After complete dissolution, 4 ml of 1M hydrochloric acid were added. Then, 8 ml of 5% sodium tetraphenylborate solution were slowly added to the solution (in about 5 minutes). After 1 hour, the white precipitate was collected on a preweight 30 ml sintered-glass filtering crucible (m1) (porosity n. 4), washed 3 times with 3 ml of 0.1% sodium tetraphenylborate solution and 2 times with 2 ml of water. The crucible was dried at 105°C until a constant weight (m2) was measured (about 24 hours). The different of weight (m2 - m1) is the total of (K,NH_4,Rb,Cs) content of the sample expressed as (K,NH_4,Rb,Cs)[$B(C_6H_5)_4$]. As the fraction of K, Rb and Cs was already known, the fraction of $(NH_4)_2O$ was calculated to be 12.7(3) wt% (Table 3).

7) Determination of CHN

Analysis of total carbon, hydrogen and nitrogen was performed using the *Leco CHN Truspec* analyser. Carbon was not detectable. Total hydrogen fraction was found to be in accordance, at a first approximation, with ammonium and water fraction of the mineral (*i.e.*, ~5.13 wt%). Unsatisfactory results were obtained for nitrogen with this method.

A representative chemical composition of boussingaultite from Pécs-Vasas is given in Table 3, and its experimental chemical formula is: $[(NH_4)_{1.77}K_{0.22})_{\Sigma 1.99}[(Mg_{0.95}Mn_{0.06})_{\Sigma 1.01}(H_2O)_{5.7}](SO_4)_{1.99}$.

8) Single-crystal neutron diffraction

8.1) *Neutron data collections and treatments*

In order to check the quality of the crystals to be used for the neutron diffraction experiments, a series of preliminary tests were performed by single-crystal X-ray diffraction with a Rigaku XtaLABSynergy-i diffractometer, equipped with a PhotonJet-i Mo*K*α microfocus source and a HyPix-6000HE Hybrid Photon Counting (HPC) detector, at the Earth Science Dept. Univ. Milan.

A single crystal with size 3.5 x 2.1 x 1.6 mm^3 was mounted on a vanadium pin of 1 mm of diameter and placed on a close-circuit displex device on the monochromatic four-circle diffractometer D19 at ILL (Grenoble, France). Neutron diffraction data were collected at 20(1) K, with a wavelength of 0.9500 Å, provided by a flat Cu monochromator using the 331 reflection, at $2\theta_M = 69.91°$ take-off angle (Gatta et al. 2021a). The measurement strategy consisted on several ω scans with steps of 0.07° at different χ and φ positions. These ω scans cover either 79° or 64° depending on the χ angle, in order to avoid collisions with the cryostat. *NOMAD* control software from ILL was used for data collection. The unit-cell determination was done by using the *PFIND* and *DIRAX* programs; processing of the raw data, to obtain the integrated intensities, was performed using the *RETREAT* and *RAFD19* programs (McIntyre and Stansfield 1988; Wilkinson et al. 1988; Duisenberg 1992). Absorption effects, due to the low-*T* device and to the crystal size and composition, were corrected using the *D19ABS* program (Matthewman et al. 1982). The lattice was found to be metrically monoclinic (Table 4, *deposited*), and consistent with the previous experimental findings of boussingaultite reported in the literature. The reflection conditions were found to be consistent with the space group $P2_1/a$. A total number of 8640 reflections were collected (with $-14 \le h \le +16$, $-17 \le k \le +21$ and $-11 \le l \le +5$), out of which 3785 were unique ($R_{int} = 0.0371$, Laue class 2/*m*) and 3463 with $F_o > 4\sigma(F_o)$, with $d_{min} \sim 0.54$ Å (Table 4, *deposited*). The Wilson plot and the statistics of distributions of the normalized structure factors suggested the structure is centrosymmetric at ~96% likelihood (with the Sheldrick's $|E^2-1|$ criterion of 0.981). Further details pertaining to neutron data collection are listed in Table 4 (*deposited*).

8.2) *Neutron structure refinements*

Anisotropic structure refinement, based on the neutron intensity data collected at 20 K, was performed using the SHELXL-2018/3 software (Sheldrick 2015) in the space group $P2_1/a$, starting from the structure model of Montgomery and Lingafelter (1964), without any H atom. Neutron scattering lengths of Mg, Mn, K, S, N, O and H were taken from Sears (1986). Secondary isotropic extinction effect was corrected according to the formalism of Larson (1967), implemented in SHELX;

however, the correction was found to be not significant. On the basis of the chemical analysis, the *Mg* site in the structure model of Montgomery and Lingafelter (1964) was modelled as partially occupied by Mg and Mn, and the fraction of the two elements was refined. After the first cycles of refinement, a series of negative residual peaks in the final difference-Fourier map of the nuclear density were found. These negative residual peaks were then assigned to ten independent H sites (*H1*, .., *H10*) in the next cycles, as H has a negative neutron scattering length. With such a structure model, convergence was achieved and the variance-covariance matrix showed no significant correlation among the refined variables. However, two significant residual peaks were found in the difference-Fourier map of the nuclear density function, only ~0.4 apart from the *O1* (*i.e.*, +4.3 fm/Å^3) and *O2* (*i.e.*, +3.4 fm/Å^3) sites and, in addition, the *N* site required a partial site occupancy for a better figure of merit. The structural model was then adjusted considering; 1) two additional O sites, labelled as *O1A* and *O2A*, with partial and refinable site occupancy, and 2) the *N* site as populated by N and K (according to the chemical analysis), and the fraction of the two elements was refined (fixing *s.o.f.*(*N*)=*s.o.f.*(*H1*,*H2*,*H3*,*H4*), Table 5 - *deposited*). With this new model, convergence was rapidly achieved and no significant correlation among the refined variables was observed in the variance-covariance matrix. The final residuals were -1.3/+0.8 fm/Å^3. All the principal mean-square atomic displacement parameters were positive (excluding the *O1A* and *O2A*, having partial site occupancy, which were modelled as isotropic) and the final $R_1(F)$= 0.0334, for 3466obs./190par. Additional details pertaining to the structure refinements with and without the split *O1A* and *O2A* sites are listed in Tables 4 (*deposited*), and the relative atomic coordinates and displacement parameters are given in Tables 5, 6 and 7 (*all deposited*) and in the CIFs. Some selected interatomic distances and angles are listed in Table 8.

Discussion and implications

The chemical data of the boussingaultite from Pécs-Vasas, obtained by the multi-methodological approach of this study, confirm the general chemical formula for this mineral reported in the literature: $(NH_4)_2[Mg(H_2O)_6](SO_4)_2$. However, two important substituents were detected: Mn^{2+} and K^+ (Table 2). The crystallographic data confirm that Mn^{2+} replaces Mg^{2+} at the octahedral *Mg* site, whereas K^+ replaces the NH_4^+ group (with K lying at the *N* site), giving the actual chemical formula: $[(NH_4)_{1.77}K_{0.22})_{\Sigma 1.99}[(Mg_{0.95}Mn_{0.06})_{\Sigma 1.01}(H_2O)_{5.7}](SO_4)_{1.99}$ (Table 3). The very low fraction of rubidium (*i.e.*, Rb_2O 0.05 wt%, Table 2) can replace NH_4^+ along with K^+, that of iron (*i.e.*, Fe_2O_3 0.01 wt%, Table 2) can replace Mg at the octahedral *Mg* site. There is no evidence of potential substituents

for the SO_4^{2-}-group. Silicon (*i.e.*, SiO_2 0.04 wt%, Table 2) is likely the effect of a low fraction of quartz coexisting with boussingaultite. The concentration of REE and other minor elements is substantially irrelevant (Tables 1 and 2). The protocol here used for the chemical analyses, and for the recalculation of the chemical formula, proved to be appropriate for such a chemically complex materials containing NH_4^+ and H_2O, which cannot be characterised using the routine protocols in mineralogy, based essentially on EPMA-WDS. We have successfully applied a similar protocol to investigate hydrous minerals containing other light elements as principal constituents, as Li, Be and B (*e.g.*, Gatta et al. 2014, 2019, 2020; Lotti et al. 2018). We cannot exclude that the slightly lower fraction of measured H_2O m.p.f.u. with respect to the ideal ones (*i.e.*, 5.7 *vs.* 6.0 m.p.f.u.) is the effect of a partial dehydration of the starting material, which is not surprising if we consider the occurrence of boussingaultite. However, the potential dehydration was not revealed by the single-crystal neutron structure refinement (based on data collected at 20 K, Table 5).

The structure model of boussingaultite obtained in this study, based on neutron diffraction data, is (partially) consistent with that of synthetic $(NH_4)_2[Mg(H_2O)_6](SO_4)_2$ previously reported by Margulis and Templeton (1962), Montgomery and Lingafelter (1964) and Maslen et al. (1988). The structure consist of three building units: isolated $Mg(H_2O)_6$-octahedra, along with isolated NH_4- and SO_4-tetrahedra connected by a complex H-bonds network (Fig. 1). Mg^{2+} is completely solvated by H_2O molecules, in a typical octahedral bonding configuration. The geometry of the $Mg(H_2O)_6$-octahedron is almost ideal, with *Mg-O* distances ranging between ~2.058 and ~2.094 Å, and *O-Mg-O* angles between ~88.70 and ~91.30°. Even the SO_4-tetrahedron is only slightly distorted, having *S-O* distances ranging between ~1.48 and ~1.49 Å and *O-S-O* between ~108.3 and ~110.1°. Isolated SO_4-tetrahedra, connected by H-bonds, usually show such an almost ideal configuration, especially at low temperature (*e.g.*, in thaumasite or in ettringite, Gatta et al. 2012, 2019). The NH_4-tetrahedron shows a modest distortion, with N-H distances and H-N-H angles ranging, respectively, between ~1.024-1.033 Å and ~106.5-111.6°. The analysis of the principal root-mean-square components of the atomic displacement parameters show that even the H sites display only a modest anisotropy: the RMS_{max}/RMS_{min} ratio is lower than 1.8 for all the seven independent *H* sites (Fig. 1, Table 7 - *deposited*). Furthermore, the H sites of the NH_4-group show a slightly higher libration anisotropy if compared to those of the H_2O molecules (Table 7 - *deposited*).

All the seven independent oxygen sites of the structure (*i.e.*, *O1*, …, *O7*, Table 5 - *deposited*) are involved in H-bonds, as *donors* or as *acceptors* (Table 8). The geometry of all the H_2O molecules, bonded to Mg, is in line with what usually observed in crystalline compounds, in which the molecules are involved in H-bonds (*e.g.*, Steiner 1998): the *O-H* distances, corrected for riding motion effect

(according to Busing and Levy 1964), range between 0.996 and 1.001 Å, the *H-O-H* angles between 105.5 and 108.2° (Table 8). The H_2O molecules show moderate-strong H-bonds, with $H\ldots O_{acceptor}$ and $O_{donor}\ldots O_{acceptor}$ ranging between 1.72-1.87 Å and 2.70-2.84 Å, respectively, along with O_{donor}-$H\ldots O_{acceptor}$ angles between 168-178° (Fig. 2, Table 8). All the H-bonds of the H_2O molecules involve the oxygen sites of the SO_4-group as *acceptors* (*i.e.*, *O1*, *O2*, *O3* and *O4*; Fig. 2, Table 8). The longest $H\ldots O_{acceptor}$ and $O_{donor}\ldots O_{acceptor}$ distances are those with *O5* as *donor* and *O4* as *acceptor* (*i.e.*, *O5…O4* = 2.836(1) and *H6…O4* = 1.870(1)), likely because *O4* is the *acceptor* of three independent H-bonds: *O5…O4*, *O6…O4* and *N…O4* (Table 8). The four independent *N-H…O* bonds show $H\ldots O_{acceptor}$ and $N_{donor}\ldots O_{acceptor}$ distances ranging between 1.81-2.00 and 2.84-2.98 Å, respectively, with *N-H…O* angles between 158-176° (Table 8). All the H-bonds of the NH_4-group involve the oxygen sites of the SO_4-group as *acceptors* (*i.e.*, *O1*, *O3* and *O4*; Fig. 2, Table 8). The SO_4-group is, therefore, the "bridging unit" between the NH_4 and the $Mg(H_2O)_6$ units, *via* H-bonds (Fig. 2, Table 8). Each of the *O-H…O* and *N-O…H* bonds involve one *donor* and one *acceptor* only; in other words, there is no evidence of bifurcated (or even trifurcated) H-bonds as found in other hydrous minerals (*e.g.*, Gatta et al. 2011, 2013, 2021b). However, some of the oxygen sites act as *donors* for more than one H-bond: this is the case of the *O1* site (*i.e.*, *N-H2…O1*, *N-H3…O1*, *O7-H10…O1*), of the *O3* site (*i.e.*, *N-H4…O3*, *O5-H5…O3*, *O7-H9…O3*), and of the *O4* site (*i.e.*, *N-H1…O4*, *O5-H6…O4*, *O6-H8…O4*) (Fig. 2, Table 8). Overall, the H-bonding network in boussingaultite is complex and pervasive, and the structure stability is expected to be substantially governed by that. This can explain previous experimental findings on the isomorphic $(NH_4)_2[Fe(H_2O)_6](SO_4)_2$, $(NH_4)_2[Zn(H_2O)_6](SO_4)_2$ or $(NH_4)_2[Co(H_2O)_6](SO_4)_2$ that showed, by *in-situ* high-temperature experiments (*i.e.*, ^1H and ^{14}N NMR, TG, DSC) the structural collapse at relatively low temperature: 320-360 K (Lim 2012; Park and Lim 2017).

The structure refinement of this study proved, unambiguously, that the partial K^+ *vs.* NH_4^+ replacement generate a local disorder. K lies at the *N* site, and its bonding configuration is that reported in Table 5 (*deposited*), describing a distorted polyhedron with CN=8 (K-O_{min} ~ 2.60 and K-O_{max}~ 3.23 Å). However, the K^+ *vs.* NH_4^+ replacement implies a change in the configuration of the SO_4 tetrahedron, through a sort of rotation of the polyhedron about the *O3-O4* vector: the *O3* and *O4* sites are kept, whereas the *O1* and *O2* sites are replaced respectively by the *O1A* and *O2A* sites, only ~0.4 Å from the parental ones, as shown in Fig. 1. Whereas the *O1A* and *O2A* are well detectable, this is not the case for the position of the *S* site of the "rotated" tetrahedron, so that only the external geometry of the rotated tetrahedron is described in Table 5 (*deposited*). The refined fraction of K^+ is 0.26 a.p.f.u., slightly higher than that obtained by chemical analysis (*i.e.*, 0.22 a.p.f.u., Table 3). To the best of our knowledge, this is the first evidence of a partial picromerite component in the boussingaultite structure, which gives rise

to a local disorder likely due to the significantly different bonding configurations of the two cations. However, the disorder does not generate any significant effect at the lattice level, as shown by the fully indexed diffraction pattern. Can the data reported in this study corroborate a potential boussingaultite-picromerite solid solution? It is not possible to answer unambiguously to this question, which requires more data with different compositions along the join. However, this study is the first step toward a better understanding of the substitution mechanisms in natural NH_4-bearing Tutton's salts. The refinement proved also that Mn^{2+} replaces Mg^{2+} at the *Mg* site. No evidence of distortion of the octahedron is observed in response to such a replacement, but the fraction of Mn^{2+} is modest. The refined fraction of Mn^{2+} is virtually identical to that obtained by the chemical analysis, *i.e.*, 0.06 a.p.f.u. (Tables 3 and 5-*deposited*). Zn^{2+}, Fe^{2+} and Ni^{2+} have already been found in isomorphic structure of boussingaultite replacing Mg^{2+}: katerinopoulosite $(NH_4)_2[Zn(H_2O)_6](SO_4)_2$, mohrite $(NH_4)_2[Fe(H_2O)_6](SO_4)_2$, and nickelboussingaultite $(NH_4)_2[Ni(H_2O)_6](SO_4)_2$. However, a Mn^{2+} member was not reported so far.

The structure model obtained in this study is consistent with the Raman and IR spectra of boussingaultite reported and interpreted by Culka et al. (2009), collected from a sample from Larderello, Tuscany, Italy (of which the chemical composition was not reported). Micro-Raman (un-oriented crystal) and IR (by diffuse reflectance infrared Fourier transform – DRIFT; powder mixed with KBr, in a ratio 1:10) spectra were described considering four main regions. The region with the highest wavenumber (*i.e.*, above 2600 cm^{-1}) displays the combination of the OH and NH_4 stretching vibrations. The region between 1800 and 1400 cm^{-1} contains the spectral signals of the NH_4 and HOH bending vibrations. The region between 1300 and 900 cm^{-1} contains the SO_4 stretching vibrations. SO_4 bending vibrations, along with the lattice modes, occur in the spectral region below 800 cm^{-1}. The assignment to each Raman and infrared bands, obtained after a deconvolution of combined signals, was proposed by the authors (Culka et al. 2009). Concerning the region of the OH and NH_4 stretching vibrations, both Raman and DRIFT spectra provide only broad bands. The deconvolution of the Raman spectrum produced a reasonable fit with four independent modes assigned to OH (*i.e.*, 3380_w, 3290_w, 3080_m, and 3040_m cm^{-1}) and two independent modes assigned to NH_4 (*i.e.*, 2919_w and 2845_w cm^{-1}). However, the peaks show different full-width-at-half-maximum (FWHM), suggesting that additional signals were likely missed (in particular at wavenumber > 3200 cm^{-1}). In the same region, the DRIFT spectrum show only a very broad band and its deconvolution led to four independent modes, two assigned to OH (*i.e.*, 3290_s and 3084_s cm^{-1}) and two to NH_4 (*i.e.*, 2913_m and 2848_m cm^{-1}). Even in this case, the occurrence of more (independent and missing) signals is highly likely. A further study, based on IR and Raman spectroscopy, was conducted on synthetic

$(NH_4)_2[Mg(H_2O)_6](SO_4)_2$ by Jayakumar et al. (1988), who reported the IR and polarized Raman spectra of the compound, with a careful assignment of the active modes coupled with a comparative analysis on what previously observed from the isomorphic $K_2[Mg(H_2O)_6](SO_4)_2$. Evidence of (coexisting) three different H_2O molecules were reported, with relative stretching and bending vibrations. The potential O_{donor}-H…$O_{acceptor}$ distances were also deduced: ranging between 0.274-0.282 Å, in good agreement with the experimental findings of this study. On the basis of the vibrational modes ascribable to the SO_4 group, the linear distortion of the tetrahedron (expressed by different *S-O* bonds) was found to be greater than its angular distortion (expressed by different *O-S-O* angles). Conversely, the NH_4 tetrahedron was found to be affected by a more pronounced angular distortion, and the possibility of free rotation of the NH_4 ion was ruled out. Even these last findings pertaining to the SO_4 and NH_4 groups are fully supported by the results of our study.

We expect that the experimental findings of this study, with a full description of the H-bonding network in boussingaultite structure, along with the libration regime and orientation of all the atomic sites (including the H sites), could led to a better modelling of its physical and chemical stability (*i.e.*, chemical reactivity in solution, phase stability under non-ambient *P/T* conditions and deformation mechanisms at the atomic scale). The full understanding of the natural occurrence of boussingaultite, and of its transformation paths in natural or industrial processes, requires the knowledge of its physical and chemical stability. In addition, this study shed new light on the mechanisms that could promote solid solution along the join boussingaultite-picromerite, and to more complex (and coexisting) substitutions in the crystalline edifice $A^{+}_2B^{2+}(SO_4)_2(H_2O)_6$ at the *A* (*e.g.*, K^+ *vs.* NH_4^+) and at the *B* (*e.g.*, Mn^{2+} *vs.* Mg^{2+}) sites.

Acknowledgements

The authors thank the Institut Laue-Langevin (Grenoble, France) for the allocation of the beamtime. GDG acknowledge the support of the Italian Ministry of Education (MIUR) through the projects 'Dipartimenti di Eccellenza 2018-2022' and 'PRIN2017 - Mineral reactivity, a key to understand large-scale processes'. The Associate Editor, O. Tschauner, the Technical Editor team and an anonymous reviewer are thanked for the revision of the manuscript.

References

Busing, W.R. and Levy, H.A. (1964) The effect of thermal motion on the estimation of bond lengths from diffraction measurements. Acta Crystallographica, 17, 142-146.

Bosi, F., Belardi, G., and Ballirano, P. (2009) Structural features in Tutton's salts $K_2[M^{2+}(H_2O)_6](SO_4)_2$, with M^{2+} = Mg, Fe, Co, Ni, Cu, and Zn. American Mineralogist, 94, 74-82.

Cipriani, C. (1958) Ricerche sulla Boussingaultite manganesifera di Larderello. Rendiconti della Società Italiana di Mineralogia e Petrologia, 14, 124.

Culka, A., Jehlička, J., and Němec, I. (2009) Raman and infrared spectroscopic study of boussingaultite and nickelboussingaultite. Spectrochimica Acta Part A: Molecular and Biomolecular Spectroscopy, 73, 420-423.

Duisenberg, A.J.M. (1992) Indexing in single-crystal diffractometry with an obstinate list of reflections. Journal of Applied Crystallography, 25, 92–96.

Ende, M., Effenberger, H., Fehér, B., Sajó, I., Kótai, L., and Szakáll, S. (2021) Kollerite, $(NH_4)_2Fe^{3+}(SO_3)_2(OH)\cdot H_2O$, a new sulfite mineral. Mitteilungen der Österreichischen Mineralogischen Gesellschaft, 167, 88.

F.A.O. (2019) World fertilizer trends and outlook to 2022. Food and Agriculture Organization of the United Nations, Rome (Italy). ISBN 978-92-5-131894-2.

Gatta, G.D., McIntyre, G.J., Sassi, R., Rotiroti, N., and Pavese, A. (2011) Hydrogen-bond and cation partitioning in $2M_1$-muscovite: A single-crystal neutron-diffraction study at 295 and 20 K. American Mineralogist, 96, 34-41.

Gatta, G.D., McIntyre, G.J., Swanson, G.J., and Jacobsen, S.D. (2012) Minerals in cement chemistry: a single-crystal neutron diffraction and Raman spectroscopic study of thaumasite, $Ca_3Si(OH)_6(CO_3)(SO_4)\cdot 12H_2O$. American Mineralogist, l97, 1060-1069.

Gatta, G.D., Merlini, M., Valdrè, G., Liermann, H-P., Nénert, G., Rothkirch, A., Kahlenberg, V., and Pavese, A. (2013) On the crystal structure and compressional behaviour of talc: a mineral of interest in petrology and material science. Physics and Chemistry of Minerals, 40, 145-156.

Gatta, G.D., Nénert, G., Guastella, G., Lotti, P., Guastoni, A., and Rizzato, S. (2014) A single-crystal neutron and X-ray diffraction study of a Li,Be-bearing brittle mica. Mineralogical Magazine, 78, 55–72.

Gatta, G.D., Hålenius, U., Bosi, F., Cañadillas-Delgado, L., and Fernandez-Diaz, M.T. (2019) Minerals in cement chemistry: A single-crystal neutron diffraction study of ettringite, $Ca_6Al_2(SO_4)_3(OH)_{12}\cdot 27H_2O$. American Mineralogist, 104, 73-78.

Gatta, G.D., Guastoni, A., Lotti, P., Guastella, G., Fabelo, O., and Fernandez-Diaz, M.T. (2019) A multi-methodological study of kurnakovite: A potential B-rich aggregate. American Mineralogist, 104, 1315-1322.

Gatta, G.D., Guastoni, A., Lotti, P., Guastella, G., Fabelo, O., and Fernandez-Diaz, M.T. (2020) A multi-methodological study of kernite, a mineral commodity of boron. American Mineralogist, 105, 1424–1431.

Gatta, G.D., Comboni, D., Fernandez-Diaz, M.T. and Fabelo Rosa, O.R. (2021a) On the labyrinthine world of natural borates: H-bonding network in probertite, $NaCaB_5O_7(OH)_4x3H_2O$; Institut Laue-Langevin (ILL), Grenoble, 2021 (DOI: 10.5291/ILL-DATA.5-11-447).

Gatta, G.D., Hradil, K., and Meven, M. (2021b) Where is the hydrogen? Elements, 17, 163-168.

Gronvold, F. and Meisingset, K.K. (1982) Thermodynamic properties and phase transitions of salt hydrates between 270 and 400 K I. $NH_4Al(SO_4)_2 \cdot 12H_2O$, $KAl(SO_4)_2 \cdot 12H_2O$, $Al_2(SO_4)_3 \cdot 17H_2O$, $ZnSO_4 \cdot 7H_2O$, $Na_2SO_4 \cdot 10H_2O$, and $Na_2S_2O_3 \cdot 5H_2O$. Journal of Chemical Thermodynamics, 14, 1083-1098.

Highfield, J., Lim, H., Fagerlund, J., and Zevenhoven, R. (2012) Activation of serpentine for CO_2 mineralization by flux extraction of soluble magnesium salts using ammonium sulfate. Royal Society of Chemistry Advances, 2, 6535.

Hofmann, W. (1931) Die Struktur der Tuttonschen Salze. Zeitschrift für Kristallographie, Mineralogie und Petrographie, 78, 279-333.

Jayakumar, V.S., Sekar, G., Rajagopal, P., and Aruldhas, G. (1988) IR and polarized Raman spectra of $(NH_4)_2Mg(SO_4)_2 \cdot 6H_2O$. Physica Status Solidi, 109, 635-640.

Larson, A.C. (1967) Inclusion of secondary extinction in least-squares calculations. Acta Crystallographica, 23, 664-665.

Larsen, E.S. and Shannon, E.V. (1920) Boussingaultite from South Mountain, near Santa Paula, California. American Mineralogist, 5, 127-128.

Li, C., Chen, X., Guo, H., Zhou, X., and Cao, J. (2020) Production of potash and N-Mg compound fertilizer via mineral shoenite from Kun Te Yi Salt Lake: Phase diagrams of the quaternary system $(NH_4)_2SO_4$-$MgSO_4$-K_2SO_4-H_2O in the isothermal evaporation and crystallization process. Acta Geologica Sinica, 95, 1016-1023.

Lim, A.R. (2012) Thermodynamic properties and phase transitions of Tutton salt $(NH_4)_2Co(SO_4)_2 \cdot 6H_2O$ crystals. Journal of Thermal Analysis and Calorimetry, 109, 1619–1623.

Lim, A.R. and Lee, J.H. (2010) ^{23}Na and ^{87}Rb relaxation study of the structural phase transitions in the Tutton salts $Na_2Zn(SO_4)_2 \cdot 6H_2O$ and $Rb_2Zn(SO_4)_2 \cdot 6H_2O$ single crystals. Physica Status Solidi, B247, 1242 - 1246.

Lotti, P., Gatta, G.D., Demitri, N., Guastella, G., Rizzato, S., Ortenzi, M.A., Magrini, F., Comboni, D., Guastoni, A., and Fernandez-Diaz M.T. (2018) Crystal-chemistry and temperature behavior of the natural hydrous borate colemanite, a mineral commodity of boron. Physics and Chemistry of Minerals, 45, 405–422.

Matthewman, J.C., Thompson, P., and Brown, P.J. (1982) The Cambridge crystallography subroutine library. Journal of Applied Crystallography, 15, 167–173.

Margulis, T.N. and Templeton, D.H. (1962) Crystal structure and hydrogen bonding of magnesium ammonium sulfate hexahydrate. Zeitschrift für Kristallographie, 117, 344-357.

Maslen, E.N., Ridout, S.C., Watson, K.J., and Moore, F.H. (1988) The structures of Tutton's salts. I. Diammonium hexaaquamagnesium(II) sulfate. Acta Crystalographica, C44, 409-412.

McIntyre, G.J. and Stansfield, R.F.D. (1988) A general Lorentz correction for single-crystal diffractometers. Acta Crystallographica, A44, 257-262.

Montgomery, H. and Lingafelter, E.C. (1964) The crystal structure of Tutton's salts. II. Magnesium ammonium sulfate hexahydrate and nickel ammonium sulfate hexahydrate. Acta Crystallographica, 17, 1478-1479.

Park, S.S. and Lim, A.R. (2017) Role of NH_4 and H_2O in Tutton salt $(NH_4)_2M(SO_4)_2 \cdot 6H_2O$ (*M*=Fe and Zn) single crystals studied by ^{1}H and ^{14}N NMR at high temperatures. Journal of the Korean Magnetic Resonance Society, 21, 67-71.

Sears, V.F. (1986) Neutron Scattering Lengths and Cross-Sections. In K. Sköld and D.L. Price, Eds., Neutron Scattering, Methods of Experimental Physics, Vol. 23A, Academic Press, New York, pp. 521-550.

Sheldrick, G.M. (2015) Crystal structure refinement with SHELXL. Acta Crystallographica Section C: Structural Chemistry, 71, 3-8.

Shimobayashi, N., Ohnishi, M., and Miura, H. (2011) Ammonium sulfate minerals from Mikasa, Hokkaido, Japan: boussingaultite, godovikovite, efremovite and tschermigite. Journal of Mineralogical and Petrological Sciences, 1103260174-1103260174.

Szabó, D., Lovász, A., Weiszburg, T., Szakáll, S., and Kristály, F. (2015) Ammonioalunite and adranosite-Al. New mineral species from the burning coal dumps of Pécs-Vasas, Hungary. Proceedings of the “6th Mineral Sciences in the Carpathians Conference”, Veszprém, Hungary, 17-19 May, 2015.

Szakáll, S. and Kristály, F. (2008) Ammonium sulphates from burning coal dumps at Komló and Pécs-Vasas, Mecsek Mts., South Hungary. Proceedings of the "2nd Central-European Mineralogical Conference (CEMS)", published in "Mineralogia, Special Papers", 32, 154.

Szakáll, S., Sajó, I., Fehér, B., and Bigi, S. (2012) Ammoniomagnesiovoltaite, a new voltaite-related mineral species from Pécs-Vasas, Hungary. Canadian Mineralogist, 50, 65-72.

Steiner, T. (1998) Opening and narrowing of the water H-O-H angle by hydrogen-bonding effects: Re-inspection of neutron diffraction data. Acta Crystallographica, B54, 464-470.

Taweepreda, W. (2013) Rubber recovery from centrifuged natural rubber latex residue using sulfuric acid. Songklanakarin Journal of Science and Technology, 35, 213-216.

Tutton, A.E.H. (1900) A comparative crystallographical study of the double selenates of the series $R_2M(SeO_4)_2 \cdot 6H_2O$. Salts in which *M* is zinc. Proceedings of the Royal Society of London, 67(435–441), 58–84.

Tutton, A.E.H. (1905) The relation of ammonium to the alkali metals. A study of ammonium magnesium and ammonium zinc sulphates and selenates. Journal of the Chemical Society, 87, 1123-1183.

Wilkinson, C., Khamis, H.W., Stansfield, R.F.D., and McIntyre, G.J. (1988) Integration of single-crystal reflections using area multidetectors. Journal of Applied Crystallography, 21, 471-478.

Table 1. REE (+Th, U) concentration by ICP-AES (see text for details).

	%m/m	ICP-AES (nm)	LOD	LOQ
Ce_2O_3	< LOD	413.764	0.003	0.01
Dy_2O_3	0.003	353.170	0.0001	0.0003
Er_2O_3	< LOD	369.265	0.002	0.007
Eu_2O_3	< LOD	381.967	0.0001	0.0003
Gd_2O_3	0.004	342.247	0.0003	0.001
Ho_2O_3	< LOD	345.600	0.0001	0.0003
La_2O_3	< LOD	398.852	0.0001	0.0003
La_2O_3	< LOD	408.672	0.0002	0.0006
Lu_2O_3	< LOD	261.542	0.0002	0.0006
Nd_2O_3	< LOD	406.109	0.0002	0.0006
Pr_2O_3	< LOD	390.844	0.0002	0.0006
Sm_2O_3	< LOD	359.260	0.0005	0.002
Sc_2O_3	< LOD	361.383	0.0005	0.002
Tb_2O_3	< LOD	350.917	0.0005	0.002
Tm_2O_3	< LOD	313.126	0.004	0.015
Yb_2O_3	< LOD	328.937	0.0001	0.0003
Y_2O_3	< LOD	371.029	0.0001	0.0003
ThO_2	< LOD	283.730	0.001	0.004
UO_2	< LOD	385.958	0.01	0.04

Note: LOD: Limit of detection (3σ); LOQ: Limit of quantification (10σ)

Table 2. Concentration of other minor elements by ICP-AES (see text for details).

	%m/m	ICP-AES (nm)		%m/m	ICP-AES (nm)
Li_2O	< 0.01	670.784	NiO	< 0.01	231.604
MgO	< 0.01	285.213	CuO	< 0.01	327.393
K_2O	2.92	766.490	Ag_2O	< 0.01	328.068
Rb_2O	0.05	780.023	ZnO	< 0.01	206.200
Cs_2O	< 0.02	852.1*	CdO	< 0.01	228.802
BeO	< 0.01	313.107	Al_2O_3	< 0.02	396.153
CaO	< 0.01	317.933	Tl_2O	< 0.02	190.801
BaO	< 0.02	233.527	PbO	< 0.05	220.353
TiO_2	< 0.01	334.940	P_2O_5	< 0.02	213.617
ZrO_2	< 0.01	343.823	As_2O_3	< 0.02	193.696
V_2O_5	< 0.02	292.464	Sb_2O_3	< 0.02	206.836
Cr_2O_3	< 0.01	267.716	Bi_2O_3	< 0.02	223.061
MoO_3	< 0.02	202.031	SiO_2	0.04	251.611
MnO	1.18	257.610	SrO	< 0.01	407.771
Fe_2O_3	0.01	238.204	B_2O_3	< 0.05	249.677
CoO	< 0.01	228.616	MgO	10.2(7)**	285.213

* by FAES; **by EDTA titration.

Table 3. Representative chemical composition of boussingaultite from Pécs-Vasas, and empirical formula recalculated on the basis of five cations.

Oxides	***Wt%***	***e.s.d.***
SO_3	44.20	± 0.20
MgO	10.60	± 0.20
$(NH_4)_2O$	12.70	± 0.30
K_2O	2.92	± 0.10
MnO	1.18	± 0.10
H_2O	28.40	± 0.20
TOTAL	100.1	

Elements	***a.p.f.u.***
S^{6+}	1.99
Mg^{2+}	0.95
NH_4^+	1.77
K^+	0.22
Mn^{2+}	0.06
H^+	11.40

Empirical formula:
$[(NH_4)_{1.77}K_{0.22})_{\Sigma 1.99}[(Mg_{0.95}Mn_{0.06})_{\Sigma 1.01}(H_2O)_{5.7}](SO_4)_{1.99}$
Ideal formula:
$(NH_4)_2[Mg(H_2O)_6](SO_4)_2$

Table 4 (*deposited*). Details of neutron data collections and refinements of boussingaultite. Ref.#1 and Ref.#2 are referred, respectively, to the refinement *without* the *O1A* and *O2A* sites and *with* the *O1A* and *O2A* sites.

	Ref. #1	Ref. #2
T (K)	20(1)	
Crystal shape	Prism	
Crystal volume (mm)	3.5 x 2.1 x 1.6	
Crystal colour	Whitish	
Unit-cell parameters	a = 9.2173(1) Å	
	b = 12.4215(3) Å	
	c = 6.2556(2) Å	
	β = 106.750(1)°	
	V = 685.83(3) Å^3	
Reference chemical formula	$(NH_4)_2[Mg(H_2O)_6](SO_4)_2$	
Space Group	$P\,2_1/a$	
Z	2	
Radiation type, λ (Å)	Neutron CW, 0.9500	
Diffractometer	D19 four-circle - ILL	
Data-collection method	ω-scans	
$d_{min.}$ (Å)	0.54	
	$-14 \le h \le +16$	
	$-17 \le k \le +21$	
	$-11 \le l \le +5$	
Measured reflections	8652	
Unique reflections	3788	
Unique reflections with $F_o > 4\sigma(F_o)$	3466	
Refined parameters	179	190
R_{Int}	0.0371	0.0371
R_σ	0.0271	0.0271
R_1 *(F)* with $F_o > 4\sigma(F_o)$	0.0456	0.0334
R_1 *(F)* for all reflections	0.0503	0.0377
$wR_2(F^2)$	0.1132	0.0801
GooF	1.614	1.143
Residuals (fm/Å^3)	-1.93/+4.28	-1.32/+0.81

Note: Statistical parameters according to the SHELXL-2018/3 definition. The two refinements were conducted using the same weighting scheme.

Table 5 (*deposited*). Refined fractional atomic coordinates and equivalent/isotropic displacement factors (Å^2) of boussingaultite, based on the neutron structure refinement at 20 K. U_{eq} is defined as one third of the trace of the orthogonalised U_{ij} tensor. *Ref.#1* and *Ref.#2* are referred, respectively, to the refinement *without* the *O1A* and *O2A* sites and *with* the *O1A* and *O2A* sites.

	Ref.#1					***Ref.#2***				
Site	*s.o.f.*	*x/a*	*y/b*	*z/c*	U_{eq}	*s.o.f.*	*x/a*	*y/b*	*z/c*	U_{eq}/U_{iso}
Mg	Mg 0.963(5), Mn 0.037(5)	0	0	0	0.0063(2)	Mg 0.947(3), Mn 0.053(3)	0	0	0	0.0063(2)
S	1	0.41004(11)	0.13300(9)	0.73463(17)	0.0058(2)	1	0.41004(8)	0.13306(7)	0.73458(12)	0.0065(1)
O1	1	0.41640(7)	0.22412(5)	0.58366(10)	0.0101(1)	0.915(6)	0.41709(10)	0.22386(5)	0.58379(7)	0.0085(2)
O1A	0					0.085(6)	0.3757(12)	0.2398(6)	0.5818(9)	0.0089(13)
O2	1	0.55141(7)	0.07043(6)	0.78275(11)	0.0126(1)	0.895(9)	0.55135(5)	0.06933(12)	0.7843(2)	0.0103(2)
O2A	0					0.105(9)	0.5519(6)	0.0945(10)	0.7497(13)	0.0095(11)
O3	1	0.28086(6)	0.06251(5)	0.61882(9)	0.00698(9)	1	0.28085(4)	0.06253(3)	0.61881(6)	0.00771(7)
O4	1	0.38669(6))	0.17482(5	0.94525(9)	0.00811(9)	1	0.38673(5)	0.17483(4)	0.94519(6)	0.00886(7)
O5	1	0.17381(6)	0.10514(5)	0.16477(9)	0.00817(9)	1	0.17383(4)	0.10513(4)	0.16480(6)	0.00892(7)
O6	1	-0.16162(6)	0.11309(5)	0.02944(9)	0.00788(9)	1	-0.16161(4)	0.11310(4)	0.02949(7)	0.00865(7)
O7	1	-0.00322(6)	-0.06902(5)	0.29772(9)	0.00767(9)	1	-0.00322(4)	-0.06900(4)	0.29778(6)	0.00833(7)
N	1	0.13458(4)	0.34231(4)	0.35306(6)	0.01071(7)	N 0.869(3), K 0.131(3)	0.13458(3)	0.34233(3)	0.35303(4)	0.00939(6)
H1	1	0.0679(2)	0.32960(18)	0.1934(3)	0.0323(4)	0.869(3)	0.06782(16)	0.32964(13)	0.1932(2)	0.0285(3)
H2	1	0.2283(2)	0.29287(17)	0.3925(4)	0.0311(3)	0.869(3)	0.22826(14)	0.29285(12)	0.3925(3)	0.0274(2)
H3	1	0.0689(2)	0.32369(19)	0.4569(3)	0.0327(4)	0.869(3)	0.06905(16)	0.32356(14)	0.4569(2)	0.0288(3)
H4	1	0.1681(2)	0.42188(15)	0.3706(3)	0.0301(3)	0.869(3)	0.16799(16)	0.42181(11)	0.3707(2)	0.0266(2)
H5	1	0.22321(17)	0.08793(14)	0.3220(2)	0.0228(2)	1	0.22316(12)	0.08793(10)	0.32201(15)	0.0235(2)
H6	1	0.25245(16)	0.12143(14)	0.0937(2)	0.0234(2)	1	0.25241(12)	0.12140(10)	0.09347(18)	0.0242(2)
H7	1	-0.26636(14)	0.09873(13)	-0.0587(2)	0.0209(2)	1	-0.26636(10)	0.09870(9)	-0.05881(17)	0.0218(2)
H8	1	-0.14189(17)	0.18806(12)	-0.0019(3)	0.0219(2)	1	-0.14187(12)	0.18804(9)	-0.00188(18)	0.0227(2)
H9	1	-0.09577(17)	-0.05940(14)	0.3425(3)	0.0233(2)	1	-0.09572(12)	-0.05947(10)	0.34248(19)	0.0242(2)
H10	1	0.02592(17)	-0.14424(12)	0.3301(2)	0.0217(2)	1	0.02595(12)	-0.14428(9)	0.33009(18)	0.0226(2)
						s.o.f.(O1)+s.o.f.(O1A) = 1, s.o.f.(O2)+s.o.f.(O2A) = 1, s.o.f.(N) = s.o.f.(H1,…, H4), *O1A* and *O2A* were modelled as isotropic				

Table 6 (*deposited*). Refined displacement parameters (Å^2) of boussingaultite in the expression: $-2\pi^2[(ha^*)^2U_{11} + \ldots + 2hka^*b^*U_{12} + \ldots + 2klb^*c^*U_{23}]$, based on the neutron structure refinement at 20 K. *Ref.#1* and *Ref.#2* are referred, respectively, to the refinement *without* the *O1A* and *O2A* sites and *with* the *O1A* and *O2A* sites.

Ref.#1	U_{11}	U_{22}	U_{33}	U_{23}	U_{13}	U_{12}
Mg	0.0056(3)	0.0063(4)	0.0066(3)	0.0002(2)	0.0010(2)	0.0001(2)
S	0.0041(3)	0.0057(4)	0.0070(3)	-0.0009(3)	0.0007(2)	-0.0009(3)
O1	0.0127(2)	0.0076(2)	0.0102(2)	0.0003(2)	0.0033(1)	-0.0029(2)
O2	0.0058(2)	0.0134(3)	0.0166(2)	-0.0036(2)	0.0002(2)	0.0017(2)
O3	0.0054(2)	0.0067(2)	0.0081(2)	-0.0009(1)	0.0007(1)	-0.0017(1)
O4	0.0099(2)	0.0065(2)	0.0073(2)	-0.0010(1)	0.0016(1)	-0.0002(1)
O5	0.0076(2)	0.0082(2)	0.0077(2)	0.0001(1)	0.0005(1)	-0.0016(1)
O6	0.0066(2)	0.0068(2)	0.0097(2)	0.0003(1)	0.0015(1)	0.0004(1)
O7	0.0081(2)	0.0069(2)	0.0082(2)	0.0007(1)	0.0027(1)	0.0004(1)
N	0.0101(1)	0.0111(2)	0.0110(1)	-0.0001(1)	0.0031(1)	-0.0003(1)
H1	0.0333(7)	0.0393(10)	0.0194(5)	-0.0025(5)	-0.0002(5)	-0.0069(7)
H2	0.0234(6)	0.0282(9)	0.0421(9)	0.0046(6)	0.0103(6)	0.0099(5)
H3	0.0318(7)	0.0415(10)	0.0306(7)	0.0068(6)	0.0184(6)	0.0037(7)
H4	0.0331(7)	0.0182(7)	0.0360(8)	-0.0013(5)	0.0050(6)	-0.0030(5)
H5	0.0232(5)	0.0274(7)	0.0146(4)	0.0028(4)	0.0004(4)	-0.0012(5)
H6	0.0198(5)	0.0287(7)	0.0241(5)	0.0002(5)	0.0103(4)	-0.0053(4)
H7	0.0132(4)	0.0214(6)	0.0253(5)	-0.0013(4)	0.0010(3)	-0.0016(4)
H8	0.0234(5)	0.0128(6)	0.0294(6)	0.0016(4)	0.0077(4)	-0.0021(4)
H9	0.0213(5)	0.0259(7)	0.0272(6)	0.0027(5)	0.0141(4)	0.0054(4)
H10	0.0256(5)	0.0144(6)	0.0256(5)	0.0039(4)	0.0083(4)	0.0041(4)

Ref.#2	U_{11}	U_{22}	U_{33}	U_{23}	U_{13}	U_{12}
Mg	0.0057(2)	0.0059(3)	0.0068(2)	0.0002(2)	0.0011(1)	0.0001(1)
S	0.0051(2)	0.0063(3)	0.0075(2)	-0.0006(2)	0.0007(2)	-0.0009(2)
O1	0.0091(3)	0.0064(2)	0.0101(2)	0.0003(1)	0.0032(1)	-0.0012(2)
O2	0.0058(2)	0.0086(4)	0.0147(3)	-0.0003(3)	0.0002(1)	0.0016(1)
O3	0.0061(1)	0.0075(2)	0.0088(1)	-0.00096(9)	0.0009(1)	-0.0016(1)
O4	0.0107(1)	0.0074(2)	0.0079(1)	-0.00095(9)	0.0017(1)	-0.0001(1)
O5	0.0082(1)	0.0090(2)	0.0084(1)	-0.0001(1)	0.0007(1)	-0.0017(1)
O6	0.0073(1)	0.0078(2)	0.0104(1)	0.0003(1)	0.0016(1)	0.0003(1)
O7	0.0088(1)	0.0075(2)	0.0089(1)	0.0008(1)	0.0028(1)	0.0004(1)
N	0.0089(1)	0.0097(1)	0.0096(1)	-0.00013(7)	0.00279(7)	-0.00037(7)
H1	0.0306(5)	0.0337(7)	0.0169(4)	-0.0021(4)	-0.0004(4)	-0.0066(5)
H2	0.0208(4)	0.0234(6)	0.0388(6)	0.0042(4)	0.0098(4)	0.0090(4)
H3	0.0285(5)	0.0363(7)	0.0270(5)	0.0060(4)	0.0166(4)	0.0030(5)
H4	0.0296(5)	0.0150(5)	0.0323(5)	-0.0012(4)	0.0042(4)	-0.0026(4)
H5	0.0238(4)	0.0285(5)	0.0150(3)	0.0029(3)	0.0005(3)	-0.0014(3)
H6	0.0207(3)	0.0295(5)	0.0248(4)	-0.0002(3)	0.0105(3)	-0.0060(3)
H7	0.0137(3)	0.0225(5)	0.0261(4)	-0.0014(3)	0.0011(2)	-0.0016(3)
H8	0.0240(4)	0.0139(4)	0.0298(4)	0.0017(3)	0.0074(3)	-0.0019(3)
H9	0.0219(3)	0.0271(5)	0.0281(4)	0.0026(3)	0.0142(3)	0.0054(3)
H10	0.0264(4)	0.0153(4)	0.0266(4)	0.0041(3)	0.0087(3)	0.0044(3)

Note: O1A and *O2A* were modelled as isotropic

Table 7 (*deposited*). Principal root-mean-square components (Å) of the atomic displacement parameters of the H sites, based on the neutron structure refinement at 20 K. *Ref.#1* and *Ref.#2* are referred, respectively, to the refinement *without* the *O1A* and *O2A* sites and *with* the *O1A* and *O2A* sites.

Ref.#1	RMS_{min}	RMS_{mid}	RMS_{max}	RMS_{max}/ RMS_{min}
H1	0.129	0.186	0.213	1.65
H2	0.124	0.186	0.208	1.68
H3	0.132	0.183	0.216	1.63
H4	0.132	0.176	0.204	1.55
H5	0.114	0.158	0.174	1.53
H6	0.118	0.158	0.177	1.50
H7	0.111	0.147	0.170	1.53
H8	0.111	0.164	0.173	1.56
H9	0.114	0.154	0.182	1.60
H10	0.113	0.156	0.168	1.49

Ref.#2	RMS_{min}	RMS_{mid}	RMS_{max}	RMS_{max}/ RMS_{min}
H1	0.121	0.173	0.202	1.68
H2	0.114	0.172	0.199	1.76
H3	0.124	0.173	0.203	1.64
H4	0.120	0.166	0.194	1.62
H5	0.116	0.160	0.178	1.53
H6	0.120	0.159	0.180	1.50
H7	0.113	0.151	0.172	1.52
H8	0.115	0.156	0.174	1.52
H9	0.117	0.158	0.185	1.58
H10	0.115	0.158	0.171	1.48

e.s.d. of RMS on the last digit

Table 8. Relevant bond distances (Å) and angles (°) based on the neutron structure refinement at 20 K. *Ref.#1* and *Ref.#2* are referred, respectively, to the refinement *without* the *O1A* and *O2A* sites and *with* the *O1A* and *O2A* sites.

Ref.#1					
Mg-O5 (x2)	2.0936(6)	*O7-Mg-O5* (x2)	88.69(2)	*O5-H5*	0.981(1)
Mg-O6 (x2)	2.0939(6)	*O7-Mg-O5'* (x2)	91.31(2)	*O5-H5**	1.001
Mg-O7 (x2)	2.0582(6)	*O7-Mg-O6* (x2)	89.79(2)	*O5...O3*	2.776(1)
		O7-Mg-O6' (x2)	90.21(2)	*H5...O3*	1.806(1)
S-O1	1.486(1)	*O5-Mg-O6* (x2)	89.94(2)	*O5-H5...O3*	169.4(1)
S-O2	1.472(1)	*O5-Mg-O6'* (x2)	90.06(2)		
S-O3	1.487(1)			*O5-H6*	0.975(2)
S-O4	1.488(1)	*O2-S-O1*	109.72(8)	*O5-H6**	0.995
		O2-S-O3	109.03(8)	*O5...O4*	2.835(1)
N-H1	1.023(2)	*O1-S-O3*	108.15(7)	*H6...O4*	1.870(1)
*N-H1**	1.0520	*O2-S-O4*	110.40(7)	*O5-H6...O4*	170.4(1)
N...O4	2.901(1)	*O1-S-O4*	109.82(8)		
H1...O4	1.925(2)	*O3-S-O4*	109.69(7)	*H5-O5-H6*	108.1(1)
N-H1 ...O4	158.3(1)				
		H1-N-H2	111.6(2)	*O6-H7*	0.980(1)
N-H2	1.030(2)	*H1-N-H3*	106.4(2)	*O6-H7**	0.998
*N-H2**	1.057	*H1-N-H4*	109.2(2)	*O6...O2*	2.703(1)
N...O1	2.971(1)	*H2-N-H3*	108.6(2)	*H7...O2*	1.723(1)
H2...O1	1.993(2)	*H2-N-H4*	109.9(2)	*O6-H7...O2*	178.4(1)
N-H2...O1	157.5(2)	*H3-N-H4*	111.0(2)		
				O6-H8	0.979(2)
N-H3	1.034(2)			*O6-H8**	0.998
*N-H3**	1.0620			*O6...O4*	2.748(1)
N...O1	2.912(1)			*H8...O4*	1.769(2)
H3...O1	1.897(2)			*O6-H8...O4*	177.5(1)
N-H3...O1	166.2(2)				
				H7-O6-H8	105.7(1)
N-H4	1.032(2)				
*N-H4**	1.0567			*O7-H9*	0.979(2)
N...O3	2.836(1)			*O7-H9**	1.001
H4...O3	1.805(2)			*O7...O3*	2.756(1)
N-H4...O3	176.0(2)			*H9...O3*	1.791(2)
				O7-H9...O3	168.1(2)
				O7-H10	0.977(2)
				*O7-H10**	0.996
				O7...O1	2.730(1)
				H10...O1	1.756(2)
				O7-H10...O1	174.3(1)
				H9-O7-H10	105.5(1)

* Bond distance corrected for "riding motion" effect, following Busing and Levy (1964)

Ref.#2					
Mg-O5 (x2)	2.0936(4)	*O7-Mg-O5* (x2)	88.70(2)	*O5-H5*	0.981(1)
Mg-O6 (x2)	2.0941(4)	*O7-Mg-O5'* (x2)	91.30(2)	*O5-H5**	1.001
Mg-O7 (x2)	2.0584(4)	*O7-Mg-O6* (x2)	89.80(2)	*O5...O3*	2.776(1)
		O7-Mg-O6' (x2)	90.20(2)	*H5...O3*	1.806(1)
S-O1	1.484(1)	*O5-Mg-O6* (x2)	89.94(2)	*O5-H5...O3*	169.48(9)
S-O2	1.479(1)	*O5-Mg-O6'* (x2)	90.06(2)		
S-O3	1.488(1)			*O5-H6*	0.975(1)
S-O4	1.488(1)	*O2-S-O1*	110.09(9)	*O5-H6**	0.996
[*S↔O1A*	1.612(8)]	*O2-S-O3*	108.67(7)	*O5...O4*	2.836(1)
[*S↔O2A*	1.370(6)]	*O1-S-O3*	108.29(5)	*H6...O4*	1.870(1)
		O2-S-O4	110.09(6)	*O5-H6...O4*	170.4(1)
K-O1A	2.603(1)	*O1-S-O4*	109.99(6)		
K-O1A'	3.279(1)	*O3-S-O4*	109.68(5)	*H5-O5-H6*	108.2(1)
K-O2	3.283(0)				
K-O2A	2.906(1)	*O3-O4*	2.433(1)	*O6-H7*	0.981(1)
K-O3	2.836(0)	*O3-O2*	2.410(1)	*O6-H7**	0.998
K-O4	2.901(2)	*O2-O1*	2.428(1)	*O6...O2*	2.703(1)
K-O5	3.232(0)	*O1-O4*	2.434(1)	*H7...O2*	1.723(1)
K-O6	3.182(1)	*O4-O3-O2*	60.28(1)	*O6-H7...O2*	178.2(1)
		O3-O2-O1	59.71(1)	*O6...O2A*	2.725(5)
N-H1	1.024(1)	*O2-O1-O4*	60.01(1)	*H7...O2A*	1.757(5)
*N-H1**	1.050	*O1-O4-O3*	59.32(1)	*O6-H7...O2A*	168.5(2)
N...O4	2.901(1)				
H1...O4	1.924(1)	*O3-O4*	2.433(1)	*O6-H8*	0.979(1)
N-H1...O4	158.3(1)	*O3-O2A*	2.427(1)	*O6-H8**	0.998
		O2A-O1A	2.453(1)	*O6...O4*	2.748(1)
N-H2	1.030(1)	*O1A-O4*	2.387(1)	*H8...O4*	1.769(1)
*N-H2**	1.055	*O4-O3-O2A*	59.88(2)	*O6-H8...O4*	177.5(1)
N...O1	2.977(1)	*O3-O2A- O1A*	59.06(2)		
H2...O1	1.999(1)	*O2A-O1A-O4*	60.13(2)	*H7-O6-H8*	105.7(1)
N-H2...O1	157.6(1)	*O1A-O4- O3*	59.87(2)		
				O7-H9	0.978(1)
N-H3	1.033(1)	*H1-N-H2*	111.6(1)	*O7-H9**	0.999
*N-H3**	1.058	*H1-N-H3*	106.5(1)	*O7...O3*	2.756(1)
N...O1	2.906(1)	*H1-N-H4*	109.2(1)	*H9...O3*	1.792(1)
H3...O1	1.892(2)	*H2-N-H3*	108.4(1)	*O7-H9...O3*	168.2(1)
N-H3...O1	166.3(1)	*H2-N-H4*	110.0(1)		
		H3-N-H4	111.0(1)	*O7-H10*	0.978(1)
N-H4	1.031(1)			*O7-H10**	0.997
*N-H4**	1.053			*O7...O1*	2.731(1)
N...O3	2.836(1)			*H10...O1*	1.757(1)
H4...O3	1.807(1)			*O7-H10...O1*	174.3(1)
N-H4...O3	175.9(1)				
				H9-O7-H10	105.5(1)

* Bond distance corrected for "riding motion" effect, following Busing and Levy (1964)

Figure 1. The crystal structure of boussingaultite, based on the neutron structure refinement of this study (intensity data collected at 20 K), viewed down [001] and [100]. Configuration of the building-block units: $Mg(H_2O)_6$-octahedron, SO_4-tetrahedron and NH_4-tetrahedron (not to scale). SO_4-tetrahedron in response to the K^+ *vs.* NH_4^+ substitution, with a sort of rotation of the polyhedron about the *O3-O4* vector: the *O3* and *O4* sites are kept, whereas the *O1* and *O2* sites are replaced respectively by the *O1A* and *O2A* sites, only ~0.4 Å from the parental ones. Displacement ellipsoid probability factor: 50%.

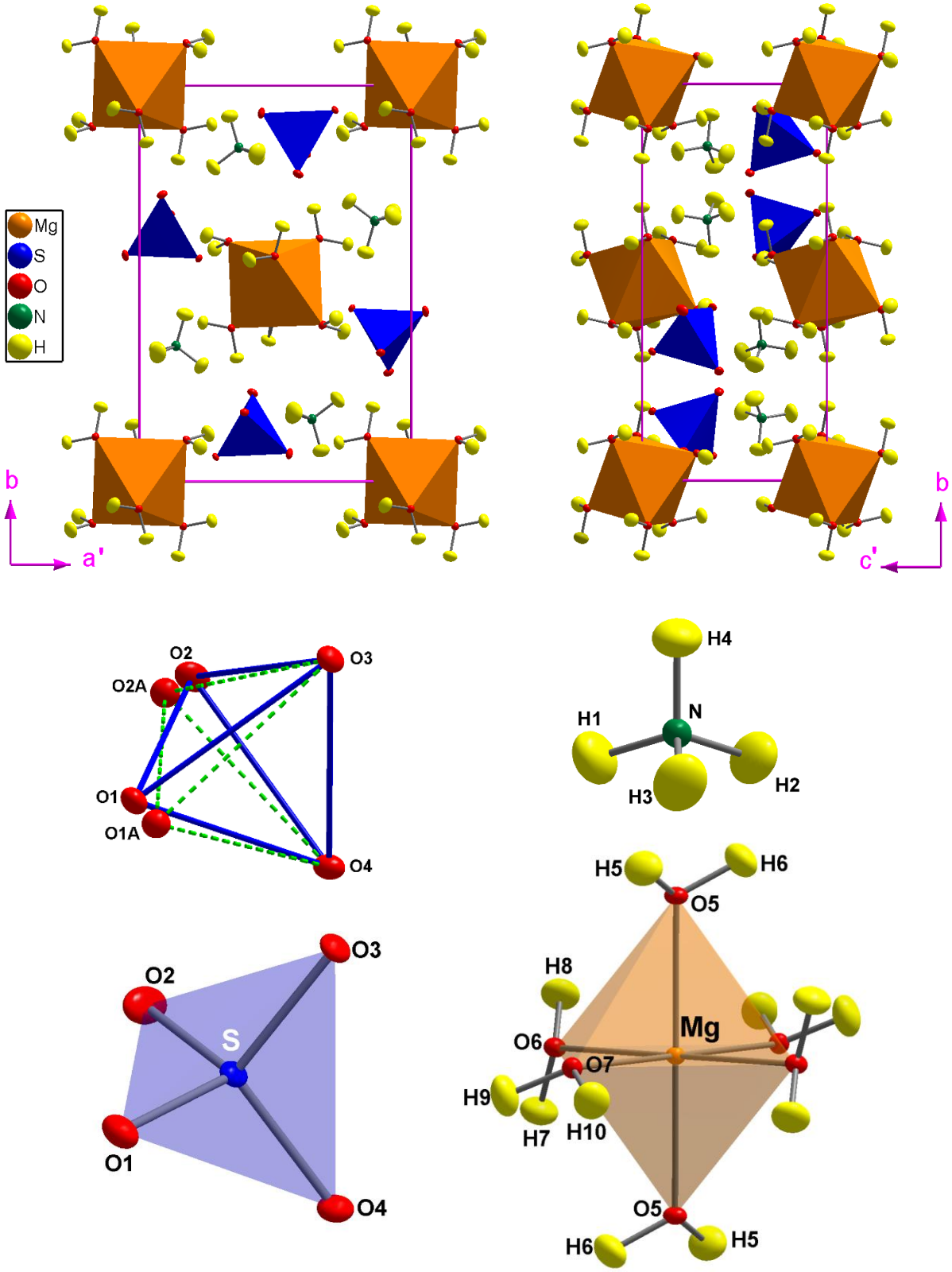

Figure 2. The complex H-bonding network into the crystal structure of boussingaultite, based on the single-crystal neutron structure refinement of this study (intensity data collected at 20 K). Details in Table 8. Displacement ellipsoid probability factor: 50%.